# OPTIMAL GROUND TARGET PATH PLANNING FOR ANGULAR RATE CONSTRAINED AGILE SATELLITE IMAGING MANEUVERS

Dennis D. Langer Norwegian University of Science and Technology 7491 Trondheim, Norway dennis.d.langer@ntnu.no

Simen Berg Norwegian University of Science and Technology 7491 Trondheim, Norway Tor A. Johansen Norwegian University of Science and Technology 7491 Trondheim, Norway Asgeir J. Sørensen Norwegian University of Science and Technology 7491 Trondheim, Norway

Abstract—Agile satellite imaging can improve coverage and image quality depending on application, for example, covering a lake with a cyanobacteria bloom event in a single push-broom image scan as opposed to several. Previous work relating to agile imaging focuses mostly on scheduling, for example by dividing point, line and area targets into straight line segments that are scheduled to be consecutively imaged. A question that is little addressed in the literature is how to define curved imaging target paths for agile push-broom imaging satellites. We present a simple approach to generate a curved imaging target path for agile imaging that considers coverage goals and an angular velocity constraint. The approach is verified by commanding the curved imaging paths to the push-broom hyperspectral imaging satellites HYPSO-1/2. The approach is able to automatically define suitable imaging paths given HYPSO-1/2's maneuvering constraints, and specified ground target and observation time.

 ${\it Index\ Terms} {\it --} {\it agile\ satellite}, path\ planning,\ optimization,\ pushbroom\ scanning$ 

#### I. INTRODUCTION

Agile Earth Observation Satellites (AEOSs) are satellites that point their remote sensing instrument towards targets of interest in three degrees of freedom, where the potential time available for imaging a target (visible time window) is larger than the time required to image a target (observation time window) [1]. This flexibility for timing the imaging of a target leads to an increase in the number of potential targets that can be imaged. For example, two targets whose imaging would overlap in time with non-agile pointing, can be made non-overlapping with agile pointing [2]. In addition, non-along track scanning enabled by continuous pointing can further increase imaging efficiency. For example, by following narrow, non-along track lying targets, as opposed to dividing such targets into multiple along track imaging strips [2].

The scope of this paper is restricted to push-broom imaging systems, which need to perform a scanning procedure to acquire and register an image with two dimensional extent. Let the line on the surface of the earth along which a push-broom system is scanning be called Imaging Target Path (ITP).

The research leading to this work has received funding from the Research Council of Norway through Grant No. 325961: Observational Pyramid with Hyperspectral Nano-Satellites for Ocean Science.

Previous literature presenting agile imaging related research focuses on methods for scheduling the imaging of many point or area targets. These targets are imaged by scanning along variable length ITP. Multiple targets are scheduled in a point-and-scan manner [1, 3]. For example, [4–6] divide area and path targets into a set of straight line ITP, that form the input to an agile imaging scheduling algorithm.

A common theme in previous work is that the atomic imaging operation is imaging along a straight line ITP, which can be either oriented parallel to the along track direction, or in some cases be oriented arbitrarily. To scan along a curved ITP, one would first approximate the target curve with a number of straight line ITPs, that are then sequentially imaged. [5] However, AEOSs are also capable of imaging maneuvers along curved ITP. Scanning along a straight line ITP that is not oriented along track already requires continuous attitude adjustment during the imaging maneuver. Hence, all satellites that perform such imaging maneuvers, could also perform maneuvers along curved ITP.

One challenge with planning such imaging maneuvers along curved ITP would be to take into account the pointing capabilities of the satellite. A high curvature ITP could require fast yaw rotations that the satellite may not be capable of. There exists little literature discussing this path planning problem for AEOS. In one instance, optimizing energy use while uniformly scanning along a given curved ITP was studied [7]. Other optimal planning research for satellite maneuvers focus on minimizing energy use or control action as the satellite transitions from one straight line ITP to the next [8, 9]. Another publication discusses scanning along curved ITP, although without considering attitude maneuvering constraints [10].

The 6 unit cubesat HYPSO-1 [11] has previously performed imaging maneuvers along a curved ITP [12]. The ITP was manually defined to cover as much of a target feature as possible with the angular velocity required to follow that path being less than the satellite's maximum angular velocity threshold. The manual definition of the curved ITP in [12] required a tuning procedure, iteratively defining and rejecting ITP that violated the angular velocity threshold until a suitable

path was found. This tuning procedure took about 30-60 minutes per capture.

In addition, once a suitable ITP is found that satisfies the constraints and the coverage goals of the planner, the ITP may not be reusable for all future observation opportunities, because the satellite azimuth and elevation angles with respect to the ground location changes depending on the satellite orbit. When considering a repetition of an imaging maneuver along a curved ITP, the path that was within the angular velocity threshold may not fall within the threshold on a subsequent observation time. The result is that the ITP would need to be manually defined again.

This motivates the following research question: How can curved ITP automatically be planned, that are robust against changing satellite imaging geometries while considering angular velocity constraints? The contribution of this paper is an answer to this research question. In addition, this paper present image data from the push-broom hyperspectral satellites HYPSO-1 and HYPSO-2 while performing imaging maneuvers along curved ITP that have been planned using the proposed method. Section II presents background information and the optimization method. Section III presents results and discussion and Section IV is the conclusion.

#### II. METHOD

#### A. Preliminaries

This paper builds upon the methods from [12]. Specifically, we use the same method for how a pointing quaternion q(t,c) is computed for a given satellite using a timestamp t and a point along a path on the surface of the earth c, and how the angular deviation between two quaternions is computed. The function q(t,c) is a non-linear function.

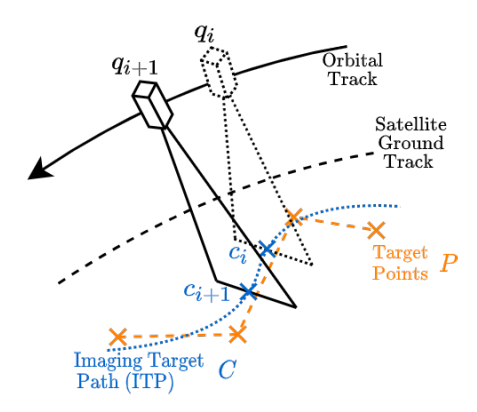


Fig. 1: Illustration of some of the terminology used.

A ground imaging target is represented as a sequence of L target points  $P=\{p_1,...p_L\}$ , that should be closely followed by the ITP on the Earth's surface. The ITP is represented as an M'th degree Bezier curve, defined with M=3 or more control points denoted as  $B=\{b_1,...,b_M\}$ . The curve is sampled at N points at uniform distance along the curve. The curve points are denoted as  $C=\{c_0,c_1,...,N_{-1}\}$ . A pointing quaternion  $q_i$  is computed for each point  $c_i$ . All N quaternions together form

a time series of attitudes called the quaternion sequence. The quaternion sequence is uploaded to the satellite and applied to its Attitude Determination and Control System (ADCS) at the rate of the ADCS control loop frequency of  $f=\frac{1}{\Delta t}$ . The relationship between N, f and the total imaging duration  $T_i$  of the scan is  $N=\lceil \frac{T_i}{f} \rceil$ . Each quaternion  $q_i$  is computed at timestamp  $t_i=T_0+i\Delta t$ , where  $T_0$  is the imaging start timestamp.

## B. Objective

The goal is to design a curved ITP that closely follows the target points, but that also takes into account the maneuverability of the satellite. The proposed objective function to achieve this goal consists of two terms: 1) A term  $O_{\omega_t}$  penalizing angular rate magnitudes above the angular velocity threshold  $\omega_t$  and 2) A term  $O_d$  penalizing distance of the ITP to the target points.

The terms are defined as follows.

$$O_{\omega_t} = \sum_{i=0}^{N-2} \max(0, \text{ rate}(q_i, q_{i+1}) - \omega_t)$$
 (1)

where dependence of  $q_i$  on  $c_i$  has been omitted.  $c_i$  is in turn derived from the control points  $b_i \in B$ , and timestamp  $t_i$ . The rate(·) function computes the average angular velocity in units of rad/s between the two quaternions using equation (14) from [12] and the relevant time step  $\Delta t$  between sample i and i+1. The  $\max(\cdot)$  function removes the contribution of smaller angular velocity values and only angular velocities above the threshold  $\omega_t$  are penalized. A penalization term in the objective function is chosen as opposed to a constraint, because short or small in magnitude angular velocities beyond this threshold may be acceptable in some cases.

The distance objective term is

$$O_d = \frac{1}{L} \sum_{i=0}^{L-1} \text{dist}(i, P, C)$$
 (2)

where the dist2 function is defined as follows

$$\operatorname{dist}(i, P, C) = \begin{cases} ||p_0, c_0||^2 & \text{if } i = 0\\ ||p_{L-1}, c_{N-1}||^2 & \text{if } i = L - 1 \\ \min_j ||p_i, c_j||^2 & \text{otherwise} \end{cases}$$
(3)

where  $||\cdot,\cdot||$  computes the Haversine distance in units of km of two geodetic coordinate points. Equation (3) computes the square of the shortest distance from the target point i to the given ITP, except for the first target point  $c_0$  and the last target point  $c_{L-1}$ . The distance squared of the first and last target points to the path are computed using respectively the first and last points of the imaging path  $c_0$  and  $c_{N-1}$ . This is to avoid the cases where the solution converges to a path that start far away from the first target point or end far away from the last target point.

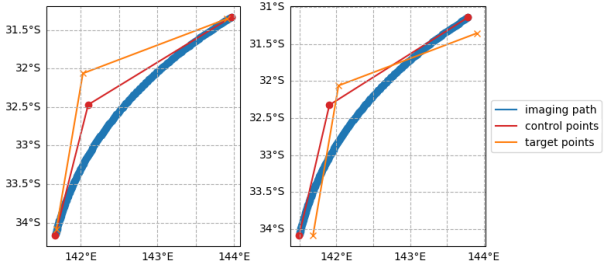
The full objective function used in optimization is the sum of the two components

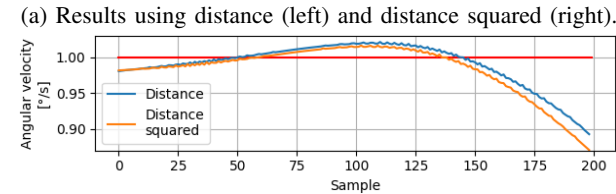
$$O = O_{\omega_{+}} + aO_{d} \tag{4}$$

where a is a tuning parameter and the optimization problem to be solved is

$$\min_{D} O \tag{5}$$

This is a non-linear, non-smooth, unconstrained optimization problem. Non-linearity is due to the computation of a quaternion from a satellite position, ground location and timestamp. Non-smoothness is due to the non-smooth functions in (1), and would favor derivative-free optimization methods.





(b) Required angular velocity scanning along the paths shown above.

Fig. 2: Illustration of the importance of using square distance in Equation (3).

See Fig. 2 for a justification for using square distance, as opposed to distance in Equation (3). The figure shows a case where the number of target points is L=3 and the imaging path is generated from a 2nd degree Bezier curve with M=3control points. The left plot in Fig. 2a shows the optimization results when using distance in Equation 3 whereas the right plot shows the results using square distance. Fig. 2b shows the angular velocities for the two cases, which are nearly identical. When using distance in Equation 3, from Fig. 2a it can be seen that the optimization solver prioritizes proximity to the first and last point over proximity to the middle point. To generate the imaging path closer to the middle point, one would either need to increase the curvature of the path and thus increase  $O_{\omega_t}$ , or translate the whole path similar to what is shown in the right plot of Fig. 2a. If the whole path is translated, then  $O_d$  would decrease once due to proximity to the middle target point, but increase twice, due to lost proximity to the first and last points, thus not decreasing the overall objective when using distance. Square distance penalizes greater distances more, leading to more balanced coverage of all target points.

Before the target points are passed to the optimization, the first and last target points are modified as follows

$$p_0' = p_0 + \alpha \frac{p_0 - p_1}{||p_0 - p_1||} \tag{6}$$

$$p'_{0} = p_{0} + \alpha \frac{p_{0} - p_{1}}{||p_{0} - p_{1}||}$$

$$p'_{L-1} = p_{L-1} + \alpha \frac{p_{L-1} - p_{L-2}}{||p_{L-1} - p_{L-2}||}$$
(6)

In effect moving the first target point back along the line from the second target towards the first target point. Similarly for the last target point. This margin is introduced to guarantee that the first and last target points are still covered in the image in case of pointing inaccuracies. For example, a pointing error of 1.0° at 600 km distance corresponds to about 10 kilometers, whose  $\alpha$  value is used in the following examples.

### III. RESULTS AND DISCUSSION

# A. Experimental setup

The objective function O is implemented as a function in the Python programming language and is minimized using the "minimize()" function from the "scipy.optimize" python package. The chosen derivative-free solver is Nelder-Mead with a tolerance parameter of  $10^{-6}$ . The control points  $b_i \in B$ are initialized as a subset of the target points P. The values for the tuning parameters in the objective function are  $a = 3/5000 \frac{\text{rad/s}}{\text{km}^2}$ 

A capture mode of HYPSO-1/2 consists of recording 598 lines at a line rate of 12 and 8 lines per second, respectively, leading to a total imaging duration of about  $T_i = 49.8 \text{ s}$ for HYPSO-1 and  $T_i = 74.75$  s for HYPSO-2. The attitude control system requires a time series of attitudes to be given at a rate of f = 4 Hz, meaning one new attitude specification every  $\Delta t = \frac{1}{f} = 0.25$  s. The manufacturer of the satellite bus recommends that the angular rate of the maneuver stays below about  $\omega_t = 1^{\circ}/s$ . This is may due to limitations of the star tracker and path following capabilities of the on-board ADCS.

#### B. Simulations and Data

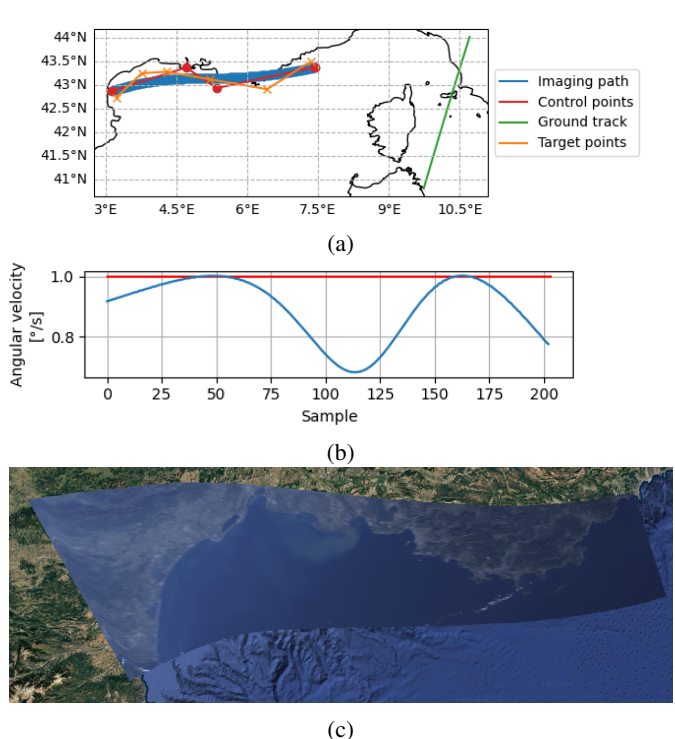


Fig. 3: "Lacrau" image. (a) target points, control points and ITP. Coastlines are shown in black. (b) angular velocity and (c) RGB composite image. Background imagery ©Google Maps

We present the results from two imaging maneuvers along curved ITP. One performed by HYPSO-1 and one performed by HYPSO-2. The satellite images shown are RGB composites of the radiance calibrated data cube and are rectified using an in-house developed georeferencing method. Both ITPs were generated from the algorithm, reducing the manual workload to only a few minutes used to define the target points.

The first image, shown in Fig. 3c, is of the Mediterranean coast of France. While the target points shown in Figure 3a follow the coastline somewhat closely, the ITP from the optimization is not following the coastline as well due to angular velocity limitations, see Fig. 3b. The ITP is about 360 km long. The satellite ground track lies about 3° longitude to the east of the target area as shown in Fig. 3a and follows roughly north to south. Scanning was done east to west. The increase in swath width and image brightness east to west indicates the growing off-nadir angle during imaging.

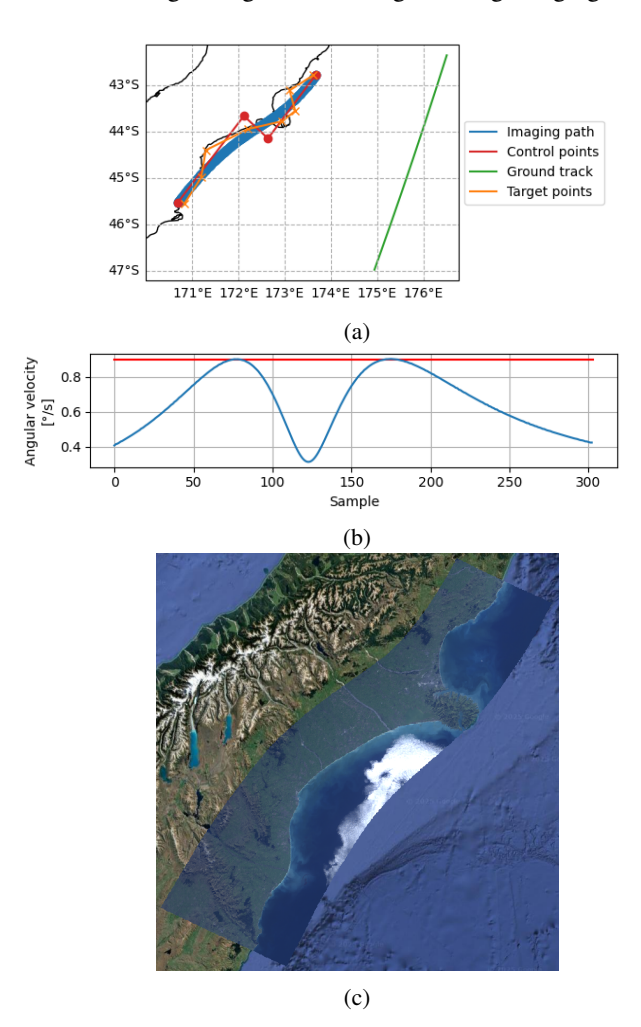


Fig. 4: "New Zealand" image. (a) satellite track, target points, control points and ITP. (b) angular velocity and (c) RGB composite image. Background imagery ©Google Maps

The second image, shown in Fig. 4c, is of the east coast of New Zealand's South Island. The ITP is about 392 km long. Because the sequence of target points are oriented more

along track than for the "Lacrau" target, there is more angular velocity budget available for yawing. Hence the slightly higher curvature in this ITP compared to Fig. 3a.

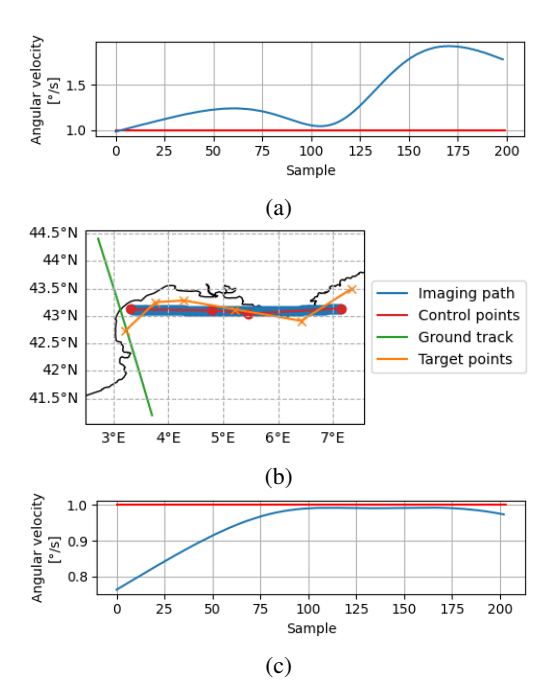


Fig. 5: Recomputing the ITP of the same target at a different observation time. (a) Angular velocity of using the previous ITP at the different observation time. (b) Recomputed ITP at the new observation time (c) Angular velocity of the new ITP.

Fig. 5a shows the angular velocity of the same ITP as in Fig. 3 computed at a different observation time. The angular velocity is above threshold due to the faster maneuvering required to follow the same ITP with the target being closer to nadir. Fig. 5b and Fig. 5c show the new ITP and its required angular velocity after the maneuver has been recomputed. The angular velocity falls below threshold again, at the expense of the ITP following the target points less closely.

### IV. CONCLUSION

The results indicate that the proposed approach is well suited for automatic generation of curved ITP along targets under angular velocity constraints. Fig. 5 in particular shows that it can also replace manual replanning at subsequent observation opportunities. Hence the proposed research question is answered. However, more work is required increase confidence in the method and solve possible issues that may emerge in not yet discovered edge cases, before it may be integrated into a fully automated satellite imaging scheduling software. For example the effect of attitude maneuvers on the output of the on-board star tracker subject to pointing exclusion zones near the earth, sun and moon, and other effects on attitude determination and control.

# REFERENCES

[1] X. Wang, G. Wu, L. Xing, and W. Pedrycz, "Agile earth observation satellite scheduling over 20 years: Formulations,

- methods, and future directions," *IEEE Systems Journal*, vol. 15, no. 3, pp. 3881–3892, Sep. 2020. [Online]. Available: https://ieeexplore.ieee.org/document/9115252
- [2] M. Lemaître, G. Verfaillie, F. Jouhaud, J.-M. Lachiver, and N. Bataille, "Selecting and scheduling observations of agile satellites," *Aerospace Science and Technology*, vol. 6, no. 5, pp. 367–381, 2002. [Online]. Available: https://www.sciencedirect. com/science/article/pii/S1270963802011732
- [3] G. Peng, R. Dewil, C. Verbeeck, A. Gunawan, L. Xing, and P. Vansteenwegen, "Agile earth observation satellite scheduling: An orienteering problem with time-dependent profits and travel times," *Computers & Operations Research*, vol. 111, pp. 84–98, 2019. [Online]. Available: https://www.sciencedirect. com/science/article/pii/S0305054819301510
- [4] Z. Lu, X. Shen, D. Li, and Y. Chen, "Integrated imaging mission planning modeling method for multi-type targets for super-agile earth observation satellite," *IEEE Journal of Selected Topics in Applied Earth Observations and Remote Sensing*, vol. 15, pp. 4156–4169, 2022. [Online]. Available: https://ieeexplore.ieee.org/document/9780007
- [5] W. Qiu, C. Xu, Z. Ren, and K. L. Teo, "Scheduling and planning framework for time delay integration imaging by agile satellite," *IEEE Transactions on Aerospace and Electronic Systems*, vol. 58, no. 1, pp. 189–205, Feb 2022. [Online]. Available: https://ieeexplore.ieee.org/document/9512262
- [6] S. Wang, L. Zhao, J. Cheng, J. Zhou, and Y. Wang, "Task scheduling and attitude planning for agile earth observation satellite with intensive tasks," *Aerospace Science and Technology*, vol. 90, pp. 23–33, 2019. [Online]. Available: https://www.sciencedirect.com/science/ article/pii/S1270963819300537
- [7] W. Qiu and C. Xu, "Attitude maneuver planning of agile satellites for time delay integration imaging," *Journal of Guidance, Control, and Dynamics*, vol. 43, no. 1, pp. 46–59, 2020. [Online]. Available: https://doi.org/10.2514/1.G003649
- [8] P. Cui, J. He, J. Cui, and H. Li, "Improved path planning and attitude control method for agile maneuver satellite with double-gimbal control moment gyros," *Mathematical Problems in Engineering*, vol. 2015, no. 1, p. 878724, 2015. [Online]. Available: https://onlinelibrary.wiley.com/doi/abs/10. 1155/2015/878724
- [9] M. Zarourati, M. Mirshams, and M. Tayefi, "Attitude path design and adaptive robust tracking control of a remote sensing satellite in various imaging modes," *Proceedings of* the Institution of Mechanical Engineers, Part G: Journal of Aerospace Engineering, vol. 237, no. 9, pp. 2166–2184, 2023. [Online]. Available: https://journals.sagepub.com/doi/10.1177/ 09544100221148887
- [10] C. Xiongzi and X. Song, "Attitude scheduling for dynamic imaging of agile earth observation satellite along a curve target," in 2018 Chinese Control And Decision Conference (CCDC), June 2018, pp. 4891–4895. [Online]. Available: https://ieeexplore.ieee.org/document/8407978
- [11] S. Bakken, M. B. Henriksen, R. Birkeland, D. D. Langer, A. E. Oudijk, S. Berg, Y. Pursley, J. L. Garrett, F. Gran-Jansen, E. Honoré-Livermore, M. E. Grøtte, B. A. Kristiansen, M. Orlandić, P. Gader, A. J. Sørensen, F. Sigernes, G. Johnsen, and T. A. Johansen, "Hypso-1 cubesat: First images and in-orbit characterization," *Remote Sensing*, vol. 15, no. 3, 2023. [Online]. Available: https://www.mdpi.com/2072-4292/ 15/3/755
- [12] D. D. Langer, J. L. Garrett, B. A. Kristiansen, S. Bakken, S. Berg, R. Birkeland, J. T. Gravdahl, T. A. Johansen, and A. J. Sørensen, "Agile maneuvers for push-broom imaging satellites," *IEEE Transactions on Geoscience and Remote Sensing*, vol. 63, pp. 1–16, 2025. [Online]. Available: https://ieeexplore.ieee.org/document/10802926